

Mechanical Properties of Resin-grouted Bolting under Thermodynamic Effect

Zhuo Yang^{1,2}

¹ Guangzhou Institute of Building Science Co., Ltd., Guangzhou 510440, China

² School of Civil Engineering, Guangzhou University, Guangzhou 510006, China

Corresponding Author Email: 165503593@qq.com

<https://doi.org/10.18280/ijht.370120>

Received: 18 August 2018

Accepted: 22 November 2018

Keywords:

resin-grouted bolting, temperature, thermodynamic effect, bolt-rock interaction

ABSTRACT

Considering the complex thermodynamic conditions in the surrounding rock of actual tunnels, this paper attempts to disclose the mechanical properties of resin-grouted bolting system under thermodynamic effect. Firstly, the mechanical properties and failure mechanism of resin-grouted bolts are examined, and the bolt-rock interaction mechanism was investigated under thermodynamic effect. On this basis, the anchoring parameters were designed under the thermodynamic effect. The results show that the failure surface of a bolt is either made of logarithmic spirals or straight lines; the elastic modulus of the bolting system is negatively linear with the temperature, while the Poisson's ratio and thermal expansion factor are positively linear with the temperature; under the constant load of 30 MPa, the yield stress of the rock sample was $87\mu\epsilon$, $95\mu\epsilon$, $105\mu\epsilon$ and $133\mu\epsilon$ at 20 °C, 40 °C, 60 °C and 80 °C, respectively; under the ideal conditions, the resin-grouted bolting system can fully offset the displacement of the surrounding rock. The research findings lay the theoretical and empirical basis for the application of resin-grouted bolting system in deep rock masses.

1. INTRODUCTION

The boom of high-rise and super-high-rise buildings has increased the risks of tunnel construction (*e.g.* ground collapse), which raises the requirements and cost of the support to foundation pit and the tunnel. The traditional support system of steel brackets cannot satisfy the latest demand for tunnel support. In tunnel construction, the surrounding rock can be reinforced and maintained through anchoring, that is, placing anchors in the boreholes on the surrounding rock. The rock bolting is an important anchoring approach. The bolts are inserted to modify the surrounding rock, forming an overall stable rock belt. The bolts work together with the surrounding rock to ensure the tunnel stability [1-4].

In China, rock bolting was first applied to coal mine tunnels, and entered the fast lane of development in the early 1990s. So far, three rock bolting methods have been developed, namely, end-anchored bolting, fully-grouted bolting and resin-grouted bolting [5]. The resin-grouted bolts are extremely easy to install. Once installed, the bolts will exert a high anchoring force, which limits the displacement of the surrounding rock [6]. However, most of resin-grouted bolts are designed based on simplified calculations. The design parameters often deviate greatly from the actual conditions, weakening the effect of rock bolting in actual projects [7-8].

In a real tunnel, the resin-grouted bolts in the surrounding rock face complex thermodynamic conditions, which arise from the internal ventilation and geothermal gradient through the tunnel. The thermodynamic effect is often so strong as to affect the anchor material (resin), thus dampening the bolting effect [9]. Under the pulling load, the bolt displacement varies with temperature, force and time. Thus, it is necessary to

explore the bolt failure mechanism under thermodynamic effect [10].

In this paper, the mechanical properties and failure mechanism of resin-grouted bolts are examined, and the bolt-rock interaction mechanism was investigated under thermodynamic effect. On this basis, the anchoring parameters were designed under the thermodynamic effect.

2. ANCHORING MECHANISM AND FAILURE TYPE

2.1 Anchoring mechanism

There are many types of resin-grouted bolts. Some bolts are grouted at the end and some are grouted fully in the borehole; some are prestressed and some are not; some are made of steel, some are made of wood and some are made of glass [11].

The bolt diameter usually falls between 16mm and 20mm. During installation, the bolt eye at the head of each bolt is bonded with resin. The commonly used steel bolts and their properties are stated in Table 1 below.

The bolts form an integrated mechanical structure with the surrounding rock. After resin-grouted bolting, the shearing or expansion of the rock mass is obstructed by the bolts when the surrounding rock faces the maximum stress. If the bolting is adopted after the breakage of the rock mass, the bolts will also withstand the pressure from the rock fragments [12, 13].

The existing theories on bolting support mainly include the suspension theory, the composite beam theory, the compound arch theory, and the loosing-circle theory of the surrounding rock [14]. There are also some less popular theories like the reduction span theory, the three-hinge arch theory, and the deformation control theory of the surrounding rock [15].

Table 1. The commonly used steel bolts and their properties

Level	Materials	Diameter	Yield Strength/MPa	Ultimate Strength/MPa	Elongation/%	
					δ_5	δ_{10}
I	Q235	6mm~40mm	260	400	26	22
II	16Mn	6mm~25mm	340	540	17	—
III	25MnSi	6mm~40mm	420	600	1430	16
	A5	6mm~40mm	300	520	—	—

2.2 Failure types

The resin-grouted bolting can enhance the lateral compressive strength, overall flexural strength and deformation modulus of the surrounding rock. Overall, three types of failure may occur to the bolting mechanism, namely, anchorage failure, long-term creep failure and tensile shear failure. The last type of failure is resulted from thermodynamic effect.

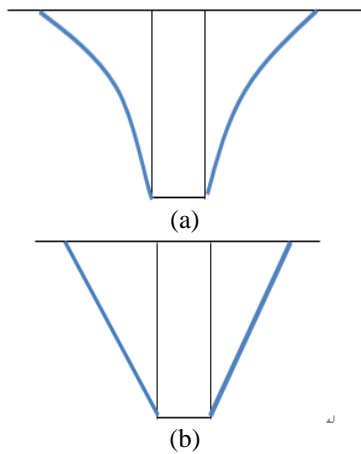


Figure 1. The shape of the failure surface of the shearing cone

The shear cone of the failure surface of a bolt is presented in Figure 1. As shown in Figures 1(a) and 1(b), the failure surface is either made of logarithmic spirals or straight lines. Thus, the bolting system is generally considered as an inverted cone to examine the shear failure. In this way, the pulling load can be derived from the shear strength of the cone.

3. MECHANICAL PROPERTIES

3.1 Thermodynamic constitutive model

Our mechanical test aims to disclose the uniaxial compressive strength, yield stress and deformation properties of the bolts grouted with unsaturated polyester resin. The parameters of the resin are listed in Table 2 below.

During the mechanical test, the temperature in the environmental chamber was increased gradually at the rate of 0.5~0.8 °C/min, and maintain constant at 20 °C, 40 °C, 60 °C and 80 °C, respectively. Each of the temperatures was kept for 1h before the start of loading. The compressive strength and yield stress of the bolting system were measured at each temperature (Table 3).

Obviously, the compressive strength and yield stress of the bolting system both decreased with the growth of temperature. The compressive strength declined by 28.42 %, 50.07 % and 54.0 %, respectively, at 40 °C, 60 °C and 80 °C.

Figures 2 and 3 respectively show the deformation parameters and the thermal expansion coefficients of the bolting system at different temperatures.

As shown in Figures 2 and 3, the Poisson’s ratio of the bolting system is positively correlated with temperature, while the elastic modulus is negatively correlated with temperature; the thermal expansion coefficient grew almost linearly with the temperature.

The structural analysis on the test results show that, due to material isotropy, the bolting system underwent viscous-elastic-plastic deformation under thermodynamic actions. The stress-strain relationship can be expressed as:

$$\sigma = \sigma_1 = \sigma_2 = \sigma_3 \tag{1}$$

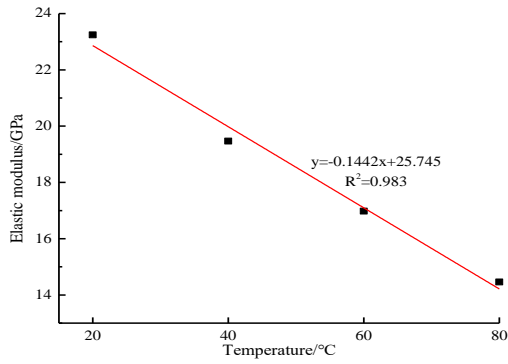
$$\varepsilon = \varepsilon_1 + \varepsilon_2 + \varepsilon_3 \tag{2}$$

Table 2. Parameters of the bolting system

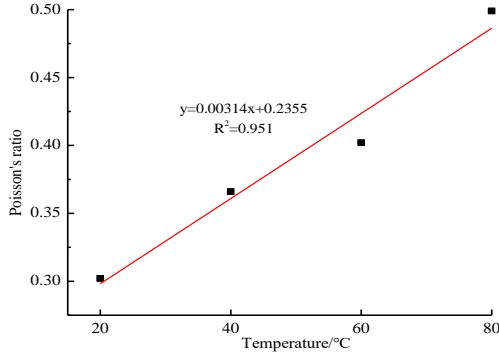
Model	Gel time/s	Carrying Time/Min	Elastic Modulus/MPa	Compressive Strength/MPa	Shear Strength/MPa
Z	90-200	50	1.2×10^4	$\sigma \geq 40 \text{MPa}$	$\tau \geq 35 \text{MPa}$

Table 3. Compressive strength and yield stress of the bolting system/MPa.

	20 °C		40 °C		60 °C		80 °C	
	σ_s	σ_c	σ_s	σ_c	σ_s	σ_c	σ_s	σ_c
Specimen 1	55.7	62.9	43.2	55.0	22.5	29.4	25.8	38.1
Specimen 2	56.3	71.2	39.4	47.5	26.4	48.8	23.7	38.9
Specimen 3	69.8	82.3	49.5	60.1	23.8	28.9	21.2	28.9
Specimen 4	70.5	79.2	37.7	48.9	26.7	38.9	17.4	27.3
Specimen 5	—	—	—	—	27.9	38.6	21.6	36.9
Mean value	63.1	73.9	42.5	52.9	25.5	36.9	21.9	34.0



(a) Elastic modulus and temperature



(b) Poisson's ratio and temperature

Figure 2. Deformation parameters of the bolting system at different temperatures

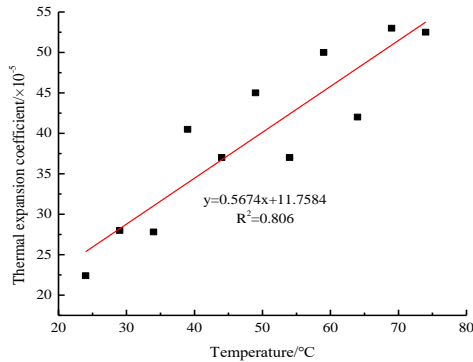


Figure 3. Thermal expansion coefficients of the bolting system at different temperatures

3.2 Tensile shear test

Under the surrounding rock stress, the tensile shear properties of the bolting system depend on the anchor length and bolt diameter. In this sub-section, a steel drum is used to simulate the surrounding rock stress, and a $\Phi 28\text{mm}$ steel cylinder was adopted to simulate the drilling into the surrounding rock. On this basis, a tensile shear test was performed on the bolting system in an environmental chamber. The outer diameter of the bolting system was 14.6mm, and each bolt was grouted to a length of 60mm. The test was carried out at four temperatures (20 °C, 40 °C, 60 °C and 80 °C), and the loading rate of 0.05 mm/s. Figure 4 shows the load-displacement curves at different temperatures.

The curves can be divided into three segments: the initial loading, the peak intensity and the residual strength, which correspond to the elastic phase, the plastic phase and the residual strength phase of shear failure.

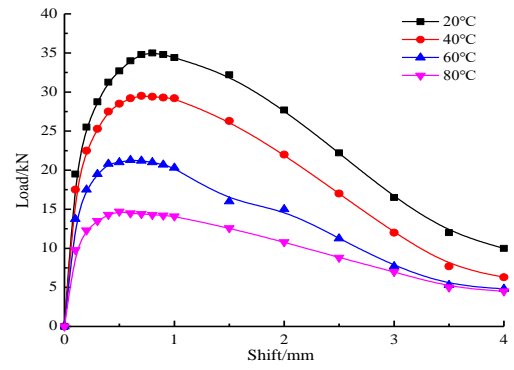


Figure 4. Load-displacement curves at different temperatures

Under the pulling stress, the displacement is positively correlated with the temperature. The load-displacement relationship can be described as:

$$\tau = K \cdot d + \zeta \quad (3)$$

where τ is the shear stress; d is the shear displacement; K is the shear stiffness; ζ is a constant

Elastic phase:

$$K_1 = \tau_1 / d_a, \zeta = 0 \quad (4)$$

where τ_1 is the ultimate tensile shear strength; d_a is the displacement under the ultimate tensile shear strength.

Plastic phase:

$$K_2 = (\tau_1 - \tau_2) / (d_a - d_b), \zeta = (\tau_2 d_a - \tau_1 d_b) / (d_a - d_b) \quad (5)$$

where τ_2 is the residual bonding strength; d_b is the displacement under the residual bonding strength.

Residual strength phase:

$$K_3 = 0, \zeta = \tau_2 \quad (6)$$

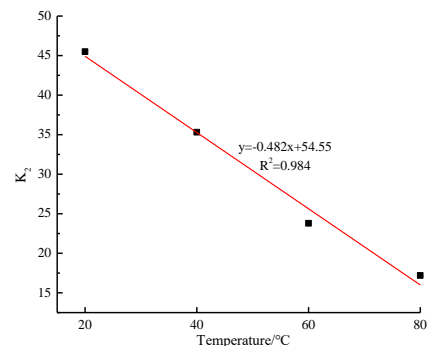
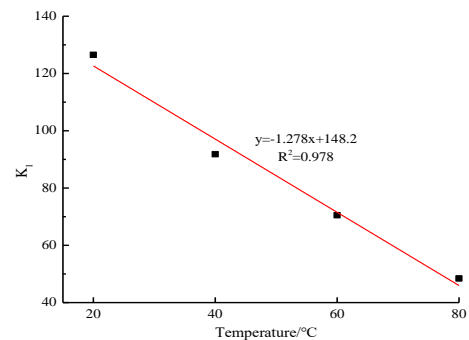


Figure 5. Relationship between tensile shear stiffness and temperature

Figure 5 shows the relationship between tensile shear stiffness and the temperature. It can be seen from Figure 5 that the tensile shear stiffness was negatively linear with the temperature in both the elastic phase and the plastic phase.

4. BOLTING EFFECT UNDER THERMODYNAMICS

4.1 Parameter design

The bolting system is usually analyzed by engineering analogy, theoretical calculation and numerical simulation. The resin-grouted area may deform under elastic and plastic mechanics. With the increase of temperature, the drawing load of the bolts in the elastic limit state decreases.

The share stress distributions of the bolts at different loads are presented in Figure 6, and the axial force distributions of the bolts at different loads are given in Figure 7.

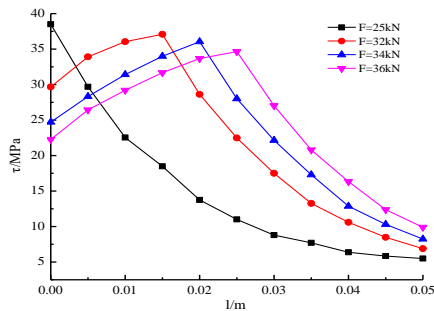


Figure 6. Shear stress distributions of the bolts at different loads

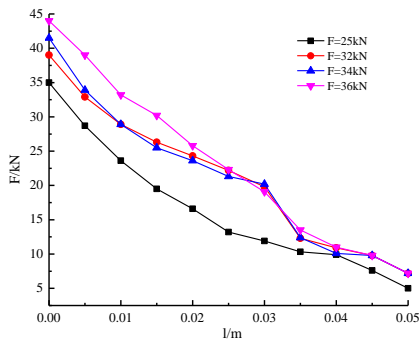


Figure 7. Axial force distributions of the bolts at different loads

As shown in Figure 6, the shear stress of the bolts gradually decreased along the axial direction, as the load climbed up to 25 kN. As the load increased to 32, 34 and 36 kN, the maximum shear stress of the bolts transferred to the farthest end of bolt. The higher the load, the longer the transfer distance.

Figure 7 shows that the axial force of the bolts decreased along the axial direction, which is different from the trend of shear stress. In addition, the axial force is positively correlated with the load.

4.2 Bolt-rock interaction

The displacement of the bolting system mainly consists of the tensile displacement of the bolts and the deformation of the surrounding rock. In the shallow rock mass, the bolting system can restrain the broken surrounding rock effectively. In the

deep rock mass, however, the bolting system may deform at a different rate with the surrounding rock, due to the high temperature gradient and high prestress of the bolts. Thus, the bolt-rock interaction mechanism should be fully explored under the thermodynamic effect. In addition, the rock mass carries different ductility and rheological properties in the shallow and deep parts under the high stress, and its Young's modulus, Poisson's ratio and tensile strength change inconsistently due to temperature variation.

In this subsection, the coring sample of surrounding rock is obtained to investigate the rheological mechanics of the rock mass under thermodynamic effect. Under the constant load of 30MPa, the yield stress of the sample was measured at 20 °C, 40 °C, 60 °C and 80 °C, respectively. The yield stresses of the sample under different temperatures are shown in Figure 8.

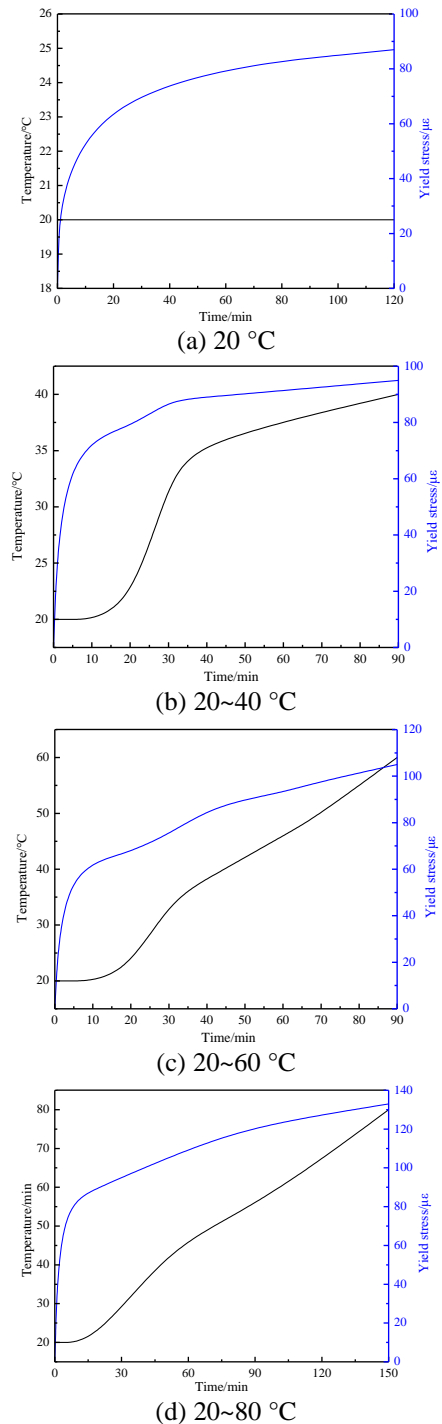


Figure 8. Yield stresses of the sample at different temperatures (Load: 30MPa)

It can be seen from Figure 8 that the yield stress of the sample increased rapidly and then slowly, and reached about $87\mu\epsilon$ after 120 min under the constant temperature of $20\text{ }^{\circ}\text{C}$; the yield stress surged up early and reached $95\mu\epsilon$ as the temperature rose to $40\text{ }^{\circ}\text{C}$; the yield stress changed similarly when the temperature increased to 60 and $80\text{ }^{\circ}\text{C}$, and stood at $105\mu\epsilon$ and $133\mu\epsilon$, respectively, under the two temperatures.

Once the bolting system is installed, both the bolts and the surrounding rock will still deform at the tunnel excavation. Since the bolts were prestressed, the bolting system will deform less than the rock. In ideal conditions, the bolt prestress can offset the rock deformation, forming a flexible support. Meanwhile, the rheological displacement of the rock at the bolt end will increase with the temperature. The sandstone has a weaker thermal effect than the mudstone. Thus, the resin-grouted bolting will have a better effect on the sandstone.

5. CONCLUSIONS

Based on the thermodynamics theory, this paper examines the mechanical properties of resin-grouted bolting system, analyses the bolt-rock interaction mechanism, and determined the anchoring parameters of the system under thermodynamic effect. The main conclusions are drawn as follows:

(1) The resin-grouted bolts are extremely easy to install. Once installed, the bolts will exert a high anchoring force, which limits the displacement of the surrounding rock. With strong anti-impact and anti-vibration effects, the resin-grouted bolting system can be applied effectively in areas under strong blasting and vibration.

(2) The resin-grouted bolting system saw a reduction in compressive strength and yield stress with the growth of temperature. For the system, the elastic modulus is negatively linear with the temperature, while the Poisson's ratio is positively linear with the temperature; the thermal expansion factor has a positive linear relationship with the temperature.

(3) The tensile shear failure of the system can be divided into the elastic phase, the plastic phase and the residual strength phase. In the first two phases, the tensile shear stiffness is negatively linear with temperature.

(4) The rock mass carries different ductility and rheological properties in the shallow and deep parts under the high stress, and its Young's modulus, Poisson's ratio and tensile strength change inconsistently due to temperature variation. The deformation of the surrounding rock can be offset by the prestress of the resin-grouted bolting system under the ideal conditions.

ACKNOWLEDGMENT

This work is supported by Guangzhou Science, Technology and Innovation Commission (Grant No.: 201803030009) and National Natural Science Foundation (Grant No. 51678171).

REFERENCES

[1] Aya S, Sasaki Y, Takezoe H. (2016). Thermodynamically anchoring-frustrated surface to trigger bulk discontinuous orientational transition. *Langmuir the Acs Journal of Surfaces & Colloids* 32(41): 10545-10555.

<https://doi.org/10.1021/acs.langmuir.6b03112>

[2] Mishra A, Zurowska M, Dabrowski R, Dhar R. (2014). Thermodynamical, electrical and electro-optical studies of a room temperature tri-component antiferroelectric liquid crystalline material. *Phase Transitions* 87(8): 746-757. <https://doi.org/10.1080/01411594.2014.893338>

[3] Aya S, Araoka F. (2017). Anomalous temperature-dependent anchoring in liquid crystals mediated by thermodynamic smectic wetting sheets. *Applied Physics Letters* 111(20): 201604. <https://doi.org/10.1063/1.4998649>

[4] Chaudhuri S, Middey A. (2014). Comparison of tropical and midlatitude thunderstorm characteristics anchored in thermodynamic and dynamic aspects. *Asia-Pacific Journal of Atmospheric Sciences* 50(2): 179-189. <https://doi.org/10.1007/s13143-014-0006-9>

[5] Lim J, Kwon YS, Park SH, Song IY, Choi J, Park T. (2011). Thermodynamic control over the competitive anchoring of n719 dye on nanocrystalline TiO_2 for improving photoinduced electron generation. *Langmuir the Acs Journal of Surfaces & Colloids* 27(23): 14647-14653. <https://doi.org/10.1021/la2026329>

[6] Fagone M, Ranocchiai G, Caggegi C, BriccoliBati S, Cuomo M. (2014). The efficiency of mechanical anchors in CFRP strengthening of masonry: An experimental analysis. *Composites Part B Engineering* 64(1): 1-15. <https://doi.org/10.1016/j.compositesb.2014.03.018>

[7] Huang W, Zhang S, Tang Y, Li Y, Nguyen L, Li Y, et al. (2016). Low-temperature transformation of methane to methanol on PD 1 o 4 single sites anchored on the internal surface of microporous silicate. *Angew Chem Int Ed Engl* 128(43): 13639-13643. <https://doi.org/10.1002/ange.201604708>

[8] Fagone M, Ranocchiai G, BriccoliBati S. (2015). An experimental analysis about the effects of mortar joints on the efficiency of anchored CFRP-to-masonry reinforcements. *Composites Part B: Engineering* 76: 133-148. <https://doi.org/10.1016/j.compositesb.2015.01.050>

[9] Xia M, Gu D, Ma C, Chen H, Zhang H. (2018). Microstructure evolution, mechanical response and underlying thermodynamic mechanism of multi-phase strengthening wc/inconel 718 composites using selective laser melting. *Journal of Alloys and Compounds* 747: 684-695. <https://doi.org/10.1016/j.jallcom.2018.03.049>

[10] Lass, Eric A. (2017). Application of computational thermodynamics to the design of a co-ni-based γ' -strengthened superalloy. *Metallurgical and Materials Transactions A* 48(5): 2443-2459. <https://doi.org/10.1007/s11661-017-4040-y>

[11] Kalfat R, Al-Mahaidi R. (2014). Experimental investigation into the size effect of bidirectional fiber patch anchors in strengthening of concrete structures. *Composite Structures* 112: 134-145. <https://doi.org/10.1016/j.compstruct.2014.02.011>

[12] Smith ST, Zhang H, Wang Z. (2013). Influence of FRP anchors on the strength and ductility of FRP-strengthened RC slabs. *Construction and Building Materials* 49: 998-1012. <https://doi.org/10.1016/j.conbuildmat.2013.02.006>

[13] Moreira S, Ramos Luis F, Oliveira DV, Louren OPB. (2014). Experimental behavior of masonry wall-to-timber elements connections strengthened with injection anchors. *Engineering Structures* 81: 98-109.

- <https://doi.org/10.1016/j.engstruct.2014.09.034>
- [14] Ludden MJW, Mulder A, Schulze K, Subramaniam V, Tampé, Robert, Huskens J. (2010). Anchoring of histidine-tagged proteins to molecular printboards: Self-assembly, thermodynamic modeling, and patterning. *Chemistry - A European Journal* 14(7): 2044-2051. <https://doi.org/10.1002/chem.200701478>
- [15] Davalos JF, Parish GC, Chen A, Ray I. (2013). Effect of anchoring schemes for beams aged by accelerated corrosion and strengthened with carbon fibre-reinforced polymer. *Structure and Infrastructure Engineering* 9(3): 229-241. <https://doi.org/10.1080/15732479.2010.542166>.